ROYAL SOCIETY OPEN SCIENCE

rsos.royalsocietypublishing.org

Research

**Cite this article:** Ma J, Zuo-Jiang SZ, He Y, Sun Q, Wang Y, Liu W, Sun S, Chen K. 2016 A facile, versatile approach to hydroxyl-anchored metal oxides with high Cr(VI) adsorption performance in water treatment. *R. Soc. open sci.* **3**: 160524. http://dx.doi.org/10.1098/rsos.160524

Received: 20 July 2016
Accepted: 14 September 2016

**Subject Category:**
Chemistry

**Subject Areas:**
materials science/environmental science

**Keywords:**
water treatment, metal oxides, adsorption, chromium

**Author for correspondence:**
Kezheng Chen
e-mail: kchen@qust.edu.cn

This article has been edited by the Royal Society of Chemistry, including the commissioning, peer review process and editorial aspects up to the point of acceptance.

THE ROYAL SOCIETY PUBLISHING

# A facile, versatile approach to hydroxyl-anchored metal oxides with high Cr(VI) adsorption performance in water treatment

Ji Ma, SiZhi Zuo-Jiang, Yunhao He, Qinglei Sun, Yunguo Wang, Wei Liu, Shuangshuang Sun and Kezheng Chen

Lab of Functional and Biomedical Nanomaterials, College of Materials Science and Engineering, Qingdao University of Science and Technology, No. 53 Zhengzhou Road, Qingdao 266042, People's Republic of China

KC, 0000-0001-6659-2078

In this study, a facile and versatile urea-assisted approach was proposed to synthesize Chinese rose-like NiO, pinecone-like ZnO and sponge-like CoO adsorbents. The presence of urea during syntheses endowed these adsorbents with high concentration of surface hydroxyl groups, which was estimated as 1.83, 1.32 and 4.19 mmol $[OH^-]\,g^{-1}$ for NiO, ZnO and CoO adsorbents, respectively. These surface hydroxyl groups would facilitate the adsorption of Cr(VI) species (e.g. $HCrO_4^-$, $Cr_2O_7^{2-}$ and $CrO_4^{2-}$) from wastewater by exchanging with hydroxyl protons or hydroxide ions, and hence result in extremely high maximum adsorbed amounts of Cr(VI), being 2974, 14 256 and 408 mg $g^{-1}$ for NiO, ZnO and CoO adsorbents in the pH range of 5.02–5.66 at 298 K, respectively. More strikingly, the maximum adsorbed amounts of Cr(VI) would be greatly enhanced as the adsorbing temperature is increased, and even amount to 23 411 mg $g^{-1}$ for ZnO adsorbents at 323 K. Based on the kinetics and equilibrium studies of adsorptive removal of Cr(VI) from wastewater, our synthetic route will greatly improve the adsorptivity of the as-synthesized metal-oxide adsorbents, and hence it will shed new light on the development of high-performance adsorbents.

## 1. Introduction

With the accelerated process of modernization, overuse of industrial chemicals, organic compounds and fossil fuels have attracted growing attention [1,2]. Abundant existence of heavy metal ions (e.g. Ba(II), Pb(II), Cd(III), Cr(III), Cr(VI), As(III), As(V),

Co(II), Cu(II), Ni(II), Zn(II) and Hg(II)) in water has become a topic of worldwide concern as it brings many severe challenges to the public health and environmental ecosystems [3,4]. Especially, the exorbitant usage and indiscriminate disposal of these metal ions in the metallurgical industry and chemical manufacturing have resulted in serious consequences. Up to now, many methods such as coagulation and flocculation [5], membrane separation [6], chemical precipitation [7], ion exchange and adsorption [8–12] have been used for removing these heavy metal ions from water bodies. Among these methods, adsorption techniques have been proved to be very effective and attractive for the purification of wastewater [13–15].

One of the most important factors in designing an adsorbent is the understanding of its adsorption mechanism. With regard to metal-oxide adsorbents, their most accepted adsorption mechanism should be the ion-exchange process reported many times in the literature [11–13,16,17]. The surface of metal oxides in aqueous solutions is hydroxylated due to dissociative chemisorption of water molecules, and the surface hydroxyl groups adsorb heavy metal ions from solution by the exchange with hydroxyl protons or hydroxide ions [18]. In this scenario, increasing the amount of surface hydroxyl groups on metal oxides will enhance ion-exchange capacity of these oxides, and hence will improve their adsorption performance in water treatment.

Along this line, a facile and versatile solvothermal approach was proposed in this work to fabricate metal oxides (including NiO, ZnO and CoO) with a high density of surface hydroxyl groups. In water treatment experiments, Cr(VI) was chosen as the adsorbate because of its high toxicity, carcinogenicity, mutagenicity to living organisms and extreme mobility [19,20]. The effluents from certain industries were reported to contain 50–100 mg $l^{-1}$ of Cr(VI), which is over 1000 times higher than the maximum allowed concentration of standard for wastewater discharge [21]. Based on our kinetics and equilibrium studies of adsorptive removal of Cr(VI) from wastewater, this approach greatly enhances the adsorptivity of metal-oxide adsorbents, and hence will shed new light on the development of high-performance adsorbents.

# 2. Material and methods

## 2.1. Syntheses of metal-oxide adsorbents

Analytical nickel sulfate ($NiSO_4 \cdot 6H_2O$), zinc acetate ($Zn(CH_3COO)_2$), cobalt nitrate ($Co(NO_3)_2 \cdot 6H_2O$), urea ($CH_4N_2O$), 1,2-propanediol, octanol and ethylene glycol were purchased from Sinopharm Chemical Reagent Co., Ltd. (China), and used as received without further purification. Typically, 2 mmol of $NiSO_4 \cdot 6H_2O$, $Zn(CH_3COO)_2$, $Co(NO_3)_2 \cdot 6H_2O$ were separately mixed with urea in a molar ratio of 1 : 1, and they were subsequently dissolved and stirred in 50 ml of 1,2-propanediol, octanol and ethylene glycol, respectively. Then these mixtures were transferred into Teflon-lined stainless-steel autoclaves with the same capacity of 100 ml for solvothermal treatment at 160°C for 24 h. The as-obtained precipitates were repeatedly washed with deionized water and ethanol, and finally dried at 60°C for 4 h.

## 2.2. Characterization

The XRD patterns were recorded on a powder X-ray diffractometer (Rigaku D/max-rA) equipped with a rotating anode and a Cu-$K_{\alpha 1}$ radiation source ($\lambda = 1.5406$ Å) at a step width of 0.02°. Scanning electron microscope (SEM) images were collected on a field-emission scanning electron microscope (JEOL JSM-6700F). The iso-electric point (IEP) of the sample was measured by testing the zeta-potential in aqueous solution on a Zetasizer Nano ZS (Malvern Instruments). Surface charge density was determined by conductometric titration method.

## 2.3. Batch adsorption experiments

Solutions with different Cr(VI) concentrations were prepared using $K_2Cr_2O_7$ as the source of heavy metal ions. For the adsorption kinetic study of Cr(VI), 40 mg of adsorbent was added into 60 ml Cr(VI) solution with initial Cr(VI) concentration of 25 mg $l^{-1}$ for different adsorbing time. To obtain the adsorption equilibrium isotherms, 20 mg of adsorbent was added into a set of 30 ml Cr(VI) solutions with different Cr(VI) concentrations, and vigorously stirred for 12 h at different temperatures. No pH buffers were used during the adsorption experiments and all the equilibrium pH values were measured between 5.02 and 5.66. After adsorption, the adsorbent was immediately separated by centrifugation from Cr(VI) solutions.

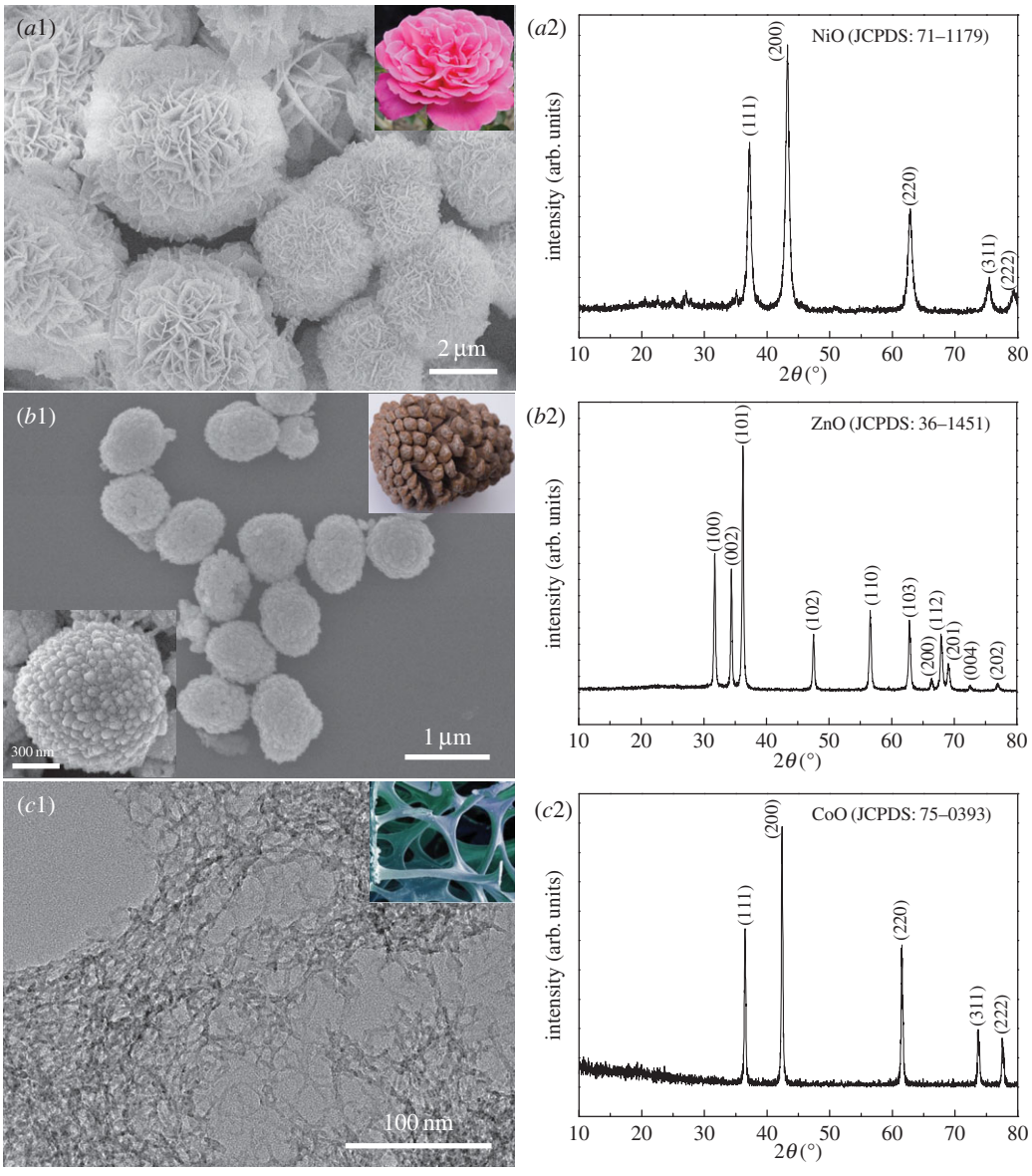


**Figure 1.** SEM images and XRD patterns of (*a*) NiO, (*b*) ZnO and (*c*) CoO adsorbents. A magnified SEM image is shown as an inset in panel *b*1, and digital photographs of Chinese rose, pinecone and sponge are shown as insets in panel *a*1, *b*1 and *c*1, respectively.

Subsequently, Cr(VI) concentrations in supernatant were determined by inductively coupled plasma-optical emission spectrometer (ICP-OES, Perkin-Elmer, Optima 8000). To investigate the effect of pH value on Cr(VI) adsorption, pH values of solutions [Cr(VI), 100 mg $l^{-1}$] before adsorbent addition were adjusted to 3, 5, 7, 9 and 11 at 298 K by adding 1 mol $l^{-1}$ HCl or NaOH solutions as needed.

## 3. Results and discussion

The morphology and chemical composition of the as-synthesized adsorbents are shown in figure 1, in which NiO (JCPDS No. 71–1179, figure 1*a*2), ZnO (JCPDS No. 36–1451, figure 1*b*2) and CoO (JCPDS No. 75–0393, figure 1*c*2) possess similar morphologies to commonplace Chinese rose, pinecone and sponge (insets in panel *a*1, *b*1 and *c*1), respectively. To be specific, the rose-like NiO architectures with a size of 3–6 µm are built from hundreds of self-assembled curving nanosheets with a thickness of about 20 nm. The pinecone-like ZnO architectures are crumpled spheroidal aggregates with an average size of *ca* 900 nm. Their particulate protuberances are not randomly assembled, as shown by a magnified SEM image in the inset of panel *b*1; instead, they are arranged along a common direction and form into the pinecone-like shape. The morphology of CoO adsorbent is akin to the sponge in our daily life, which is of open network structure assembled by interconnected nanofibres. According to the Scherrer equation,

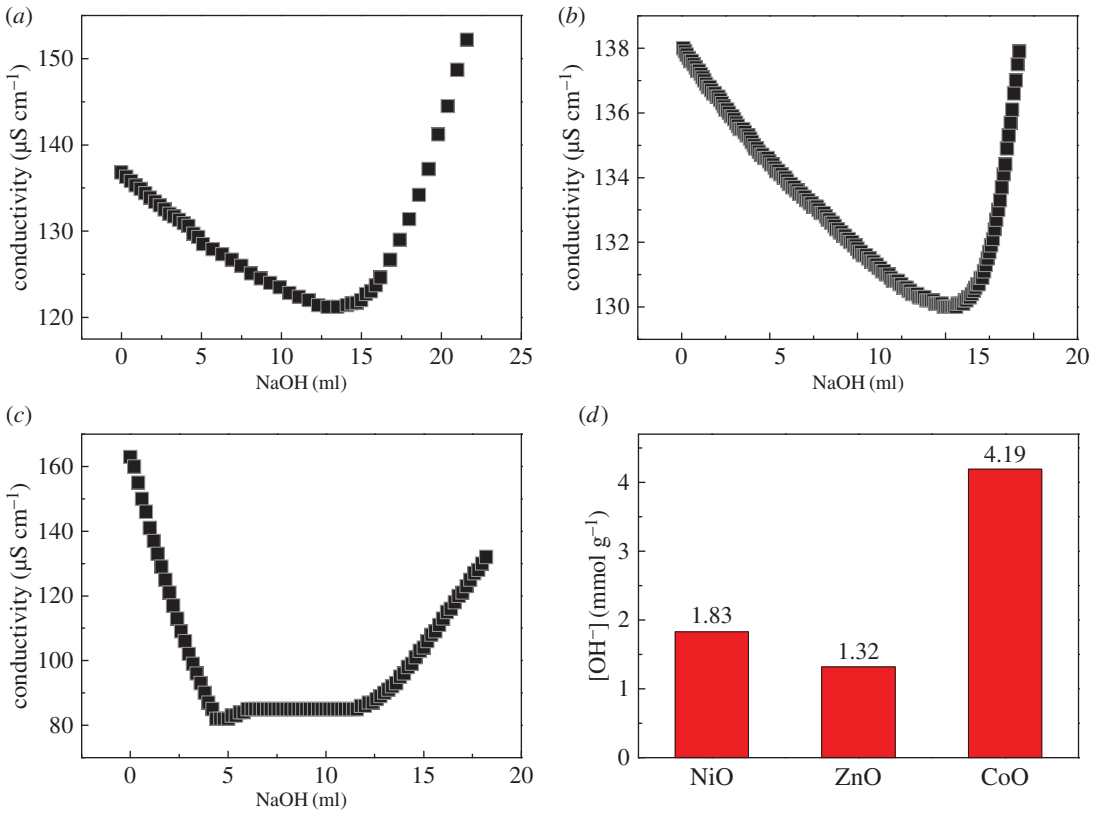


**Figure 2.** Conductometric titration of (*a*) NiO, (*b*) ZnO and (*c*) CoO adsorbents. (*d*) Surface charge density [$OH^-$] of these adsorbents.

the average crystallite sizes are calculated to be *ca* 12.8, 29.5 and 32.4 nm for rose-like NiO, pinecone-like ZnO and sponge-like CoO products, respectively, determined from (200), (111) peaks for NiO, (101), (100) peaks for ZnO, and (200), (111) peaks for CoO.

The facile syntheses of these NiO, ZnO and CoO adsorbents with well-defined morphologies share a common feature of the usage of urea during their solvothermal reactions. Generally, urea acts as a chelating agent of metal ions and in this way prevents their aggregation [22]. This peculiarity of urea can thus provide fine control of the final morphologies of these metal-oxide adsorbents. Most notably, the urea-involved hydrothermal procedure has been found to exhibit lower Lewis acidity, but higher concentration of surface hydroxyl groups [23]. To verify this point, the surface charge densities of these NiO, ZnO and CoO adsorbents were measured by conductometric titration method. In a typical measurement, 10 mg of the adsorbent was firstly dispersed into 100 ml of de-ionized water and stirred with a magnetic bar. After adding a certain amount of hydrochloric acid, the solution was titrated with sodium hydroxide (5 mmol $l^{-1}$) and meanwhile the conductivity was recorded (figure 2*a–c*). Figure 2*d* shows that the calculated surface hydroxyl densities are 1.83, 1.32 and 4.19 mmol [$OH^-$] $g^{-1}$ with regard to NiO, ZnO and CoO adsorbents, respectively. These values are extremely large and probably due to the usage of urea in our experiments. In this scenario, $Cr_2O_7^{2-}$/$HCrO_4^-$ anions in wastewater will exchange with these numerous hydroxyl groups to promote the chemisorption process [11,16,17], and hence greatly improve the adsorptive capacity of these adsorbents. It should be mentioned that these surface hydroxyl densities are seemingly irrelevant to the crystallite sizes of NiO, ZnO and CoO, revealing that the assembling manner of primary particles has a critical impact on the number of their surface hydroxyl groups.

Figure 3*a* shows the kinetics of Cr(VI) adsorption onto NiO, ZnO and CoO adsorbents with an initial concentration of 25 mg $l^{-1}$ at 298 K. Generally, the adsorption equilibrium of Cr(VI) on these metal-oxide adsorbents was achieved within 30 min. The pseudo-second-order kinetic model was used to fit these experimental data (figure 3*b*), and the obtained parameters are summarized and listed in table 1. The high correlation coefficients ($R^2$) of *ca* 0.99 indicate a good description of these kinetic data by this pseudo-second-order model. More strikingly, the initial adsorption rates $h$, which can be determined by $h = kq_e^2$ (where $k$ is the rate constant (g $mg^{-1}$ $min^{-1}$), $q_e$ is the equilibrium adsorption capacity (mg $g^{-1}$)), are

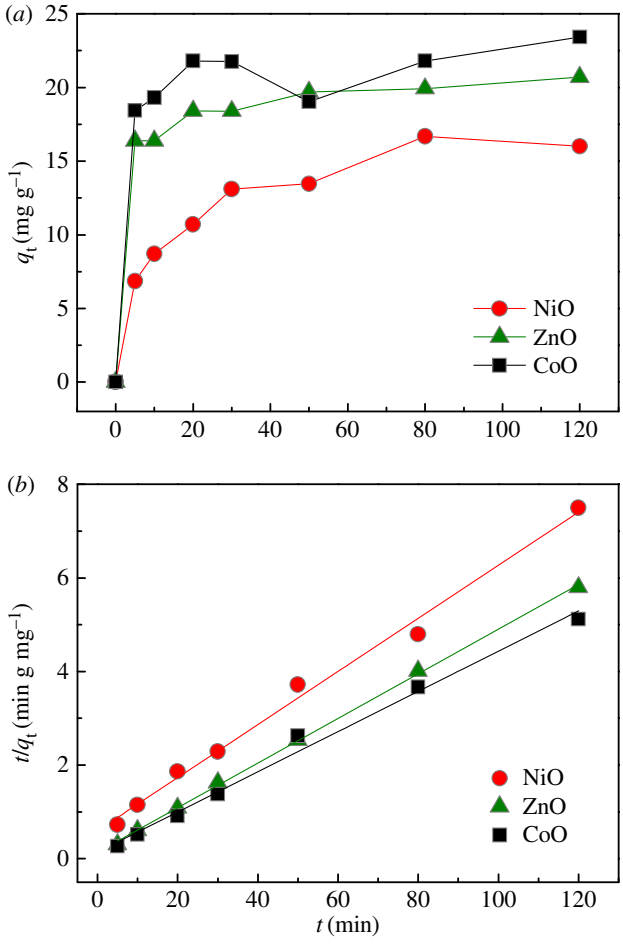


**Figure 3.** (*a*) The kinetics of Cr(VI) adsorption onto NiO, ZnO and CoO adsorbents with an initial concentration of 25 mg l$^{-1}$ at 298 K. (*b*) Linear plots of the data in panel *a* based on the pseudo-second-order model.

**Table 1.** Fitted parameters of Cr(VI) adsorption kinetics based on pseudo-second-order model.

| adsorbents | $k$ (g mg$^{-1}$ min$^{-1}$) | $q_e$ (mg g$^{-1}$) | $h$ (mg g$^{-1}$ min$^{-1}$) | $R^2$ |
|---|---|---|---|---|
| NiO | 0.0054 | 17.63 | 1.68 | 0.991 |
| ZnO | 0.0163 | 20.99 | 7.18 | 0.999 |
| CoO | 0.0133 | 23.28 | 7.21 | 0.990 |

above 7.0 mg g$^{-1}$ min$^{-1}$ for ZnO and CoO adsorbents, which meet the requirements of 'quick water-treatment' in industry.

The adsorption isotherms of Cr(VI) on NiO, ZnO and CoO adsorbents at different temperatures are shown in figure 4. Most strikingly, the adsorbed amounts of Cr(VI) increase fast at any given Cr(VI) concentration. The Langmuir [24] and Freundlich [25] models were then used to fit these isotherm data, and the fitted parameters are summarized and listed in table 2. The high $R^2$-values, being very close to or even equal to unity, indicate that the Langmuir and Freundlich models can both describe the adsorption isotherms in this study. The Langmuir isotherm model provides a unitless constant separation factor $R_L$, defined by $R_L = (1 + K_L C_0)^{-1}$ [26], wherein $K_L$ is the Langmuir adsorption constant related to the affinity of binding sites (l mg$^{-1}$) and $C_0$ is initial concentration of Cr(VI) (mg l$^{-1}$). The value of $R_L$ indicates the types of Langmuir isotherm of irreversible ($R_L = 0$), favourable ($0 < R_L < 1$), linear ($R_L = 1$) or unfavourable ($R_L > 1$). By calculation, $R_L$ is between 0 and 1 for all adsorbents at any initial Cr(VI) concentration, indicative of the favourable Langmuir isotherm in this study. According

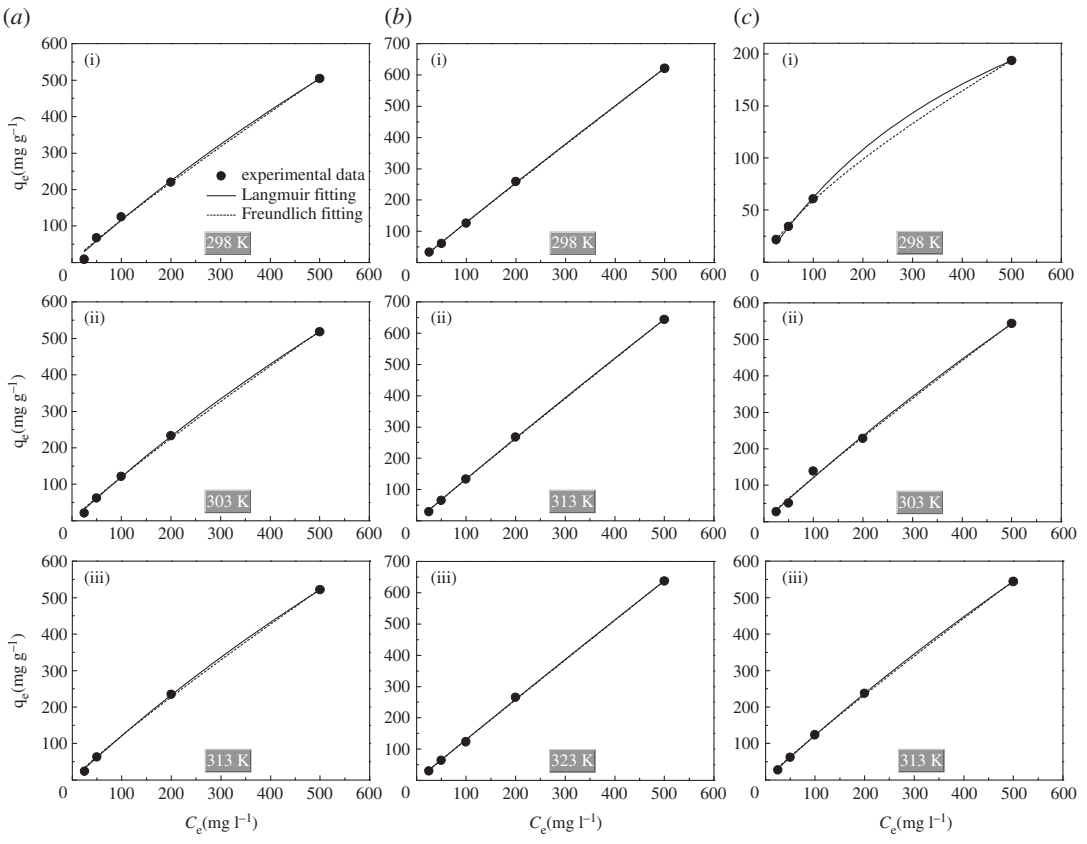


**Figure 4.** Adsorption isotherms of Cr(VI) on (*a*) NiO, (*b*) ZnO and (*c*) CoO adsorbents at different temperatures.

**Table 2.** Fitted parameters of Cr(VI) adsorption isotherms for NiO, ZnO and CoO adsorbents at different temperatures.

| | | Langmuir model | | | Freundlich model | | |
|---|---|---|---|---|---|---|---|
| adsorbents | $T$ (K) | $K_L$ (l mg$^{-1}$) | $q_m$(mg g$^{-1}$) | $R^2$ | $K_F$ ((mg g$^{-1}$) (l mg$^{-1}$)$^{1/n}$) | $n$ | $R^2$ |
| NiO | 298 | 0.000408 | 2973.70 | 0.995 | 1.752 | 1.097 | 0.994 |
| | 303 | 0.000424 | 2961.71 | 0.999 | 1.827 | 1.100 | 0.998 |
| | 313 | 0.000426 | 2968.88 | 0.999 | 1.865 | 1.103 | 0.998 |
| ZnO | 298 | 0.0000911 | 14 255.88 | 1.000 | 1.404 | 1.020 | 1.000 |
| | 313 | 0.0000910 | 14 807.61 | 1.000 | 1.455 | 1.020 | 1.000 |
| | 323 | 0.0000560 | 23 411.79 | 0.999 | 1.353 | 1.009 | 0.999 |
| CoO | 298 | 0.0018 | 408.37 | 0.998 | 2.006 | 1.360 | 0.999 |
| | 303 | 0.000296 | 4208.80 | 0.996 | 1.676 | 1.075 | 0.996 |
| | 313 | 0.000321 | 3936.82 | 1.000 | 1.719 | 1.079 | 0.999 |

to the Langmuir fitting results, the maximum adsorbed amounts ($q_m$) of Cr(VI) are about 2974, 14 256 and 408 mg g$^{-1}$ for NiO, ZnO and CoO adsorbents at 298 K, respectively. As adsorbing temperature is elevated, the $q_m$ value progressively increases in the case of ZnO and CoO adsorbents, while it remains stable for the NiO adsorbent. The strong upward trend of $q_m$ values regarding ZnO and CoO adsorbents verifies the presence of chemisorption process (i.e. ion-exchange reaction) in water treatment. By contrast, the nearly unchanged $q_m$ values of the NiO adsorbent at any given temperature indicate the presence of other determinants, which will be discussed later. It is noteworthy that most of these $q_m$

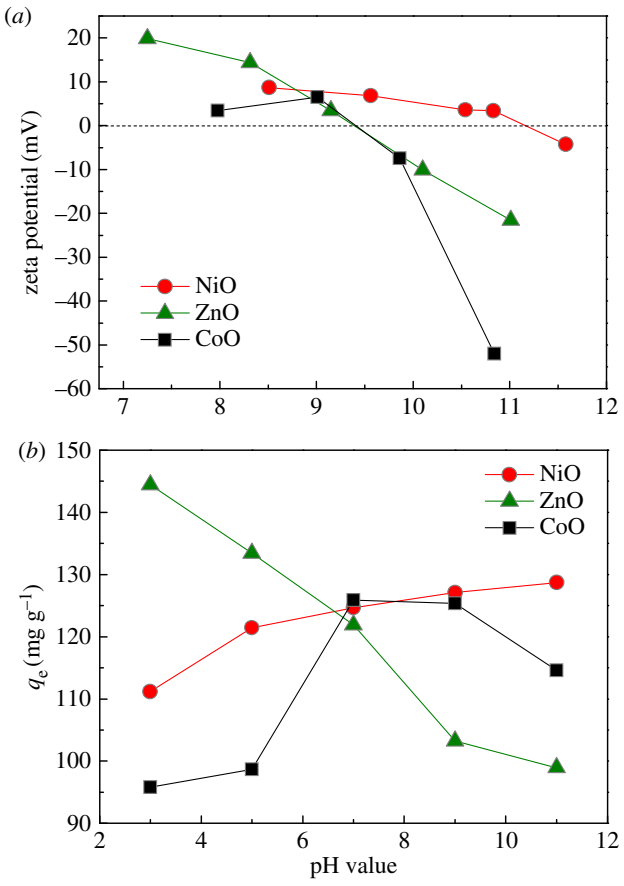


**Figure 5.** (*a*) pH-dependent zeta potential values of NiO, ZnO and CoO adsorbents in aqueous solution at 298 K. (*b*) Effect of pH values on the equilibrium adsorption capacity for these adsorbents with initial Cr(VI) concentration of 100 mg l$^{-1}$ at 298 K.

values rival or even surpass the reported values in the literature [27–29], strongly evidencing that our versatile urea-assisted approach is remarkably advantageous in synthesizing hydroxyl-anchored metal-oxide adsorbents with high Cr(VI) adsorption performance. On the other hand, the Freundlich model describes the adsorption on an energetically heterogeneous surface on which the adsorbed molecules are interactive. The Freundlich constants $K_F$ ((mg g$^{-1}$)(l mg$^{-1}$)$^{1/n}$) and $n$ (unitless) are related to the adsorbed amount and adsorption affinity, respectively. The values of $1/n$ are less than 1 for all Cr(VI) adsorbents, indicating the degree of nonlinearity between the solution concentration and amount of Cr(VI) ions adsorbed [30].

To seek deep insight into the extremely high adsorptive capacity of these hydroxyl-anchored metal-oxide adsorbents, IEP values were determined by measuring pH-dependent zeta-potential values in aqueous solution. It is clearly observed from figure 5*a* that the IEP values can be estimated as 11.2, 9.4, 9.4 for NiO, ZnO, CoO adsorbents, respectively. The pH dependence of their equilibrium adsorption capacity is shown in figure 5*b*. As is known, Cr(VI) exists mainly in the soluble forms of both $HCrO_4^-$ and $Cr_2O_7^{2-}$ at pH from 2.0 to 6.5 [20,26], and $HCrO_4^-$ and $Cr_2O_7^{2-}$ anions account for about 80% and 20%, respectively, in the pH range of 2–5 [31]. As the pH value increases above 6.5, Cr(VI) exists mainly in soluble form of $CrO_4^{2-}$ [26]. Based on the above discussion, when the pH value is below the IEP values of these three adsorbents, the positive surface charge would electrostatically attract the Cr(VI) species ($HCrO_4^-$, $Cr_2O_7^{2-}$ and $CrO_4^{2-}$) to enhance the adsorptive capacity of the adsorbent (e.g. ZnO case in figure 5*b*); alternatively, the excess $H^+$ cations in solution may also lower the surface hydroxyl site densities on the adsorbent, and hence reduce the ion-exchange ability and adsorptive capacity of the adsorbent (e.g. NiO and CoO cases in figure 5*b*). At high pH values above the IEP values, the deprotonation of adsorbent's surface can facilitate the electrostatic repulsion between the adsorbent and Cr(VI) species (mainly $CrO_4^{2-}$) to reduce its adsorptive capacity (e.g. ZnO and CoO case in figure 5*b*).

Although the NiO, ZnO and CoO adsorbents exhibit different pH-dependent adsorption behaviours, their facile and versatile syntheses and high adsorptive capacity for Cr(VI) ions are most attractive in practical water treatment. Before that, these metal-oxide adsorbents have to be evaluated in at least

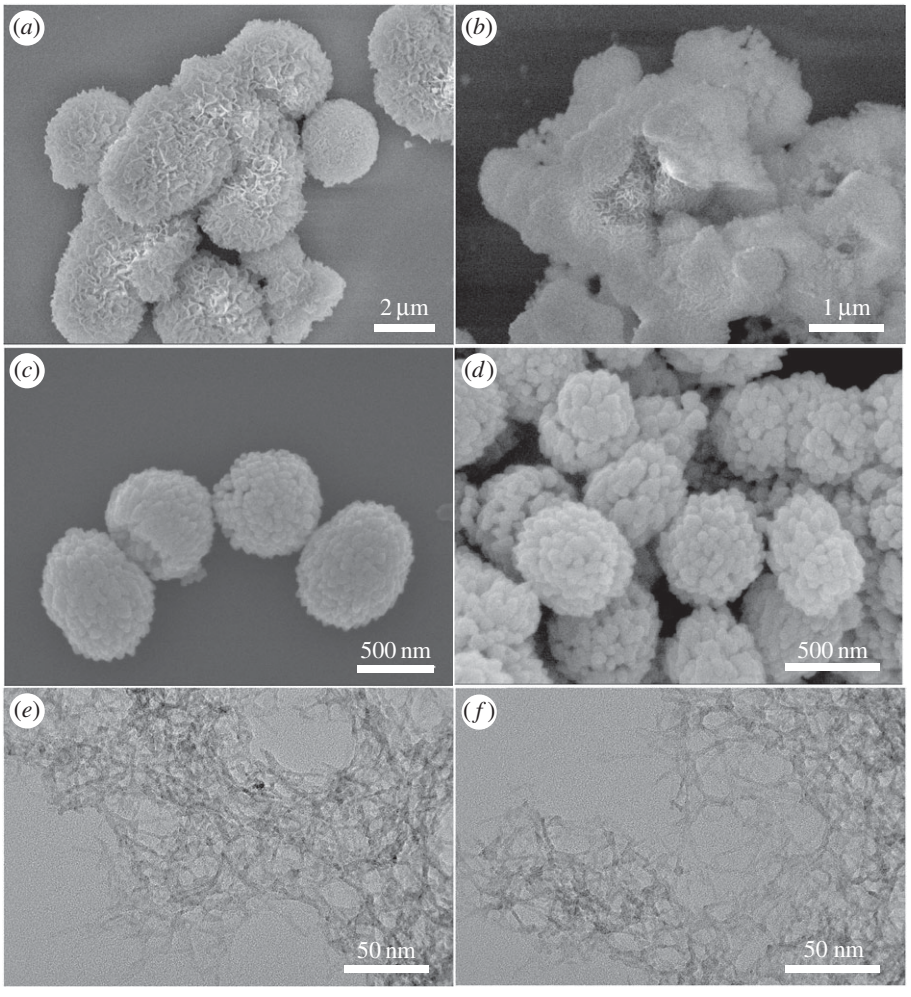


**Figure 6.** SEM images of (*a*,*b*) NiO, (*c*,*d*) ZnO, and TEM images of (*e*,*f*) CoO adsorbents after Cr(VI) adsorption (panels *a*,*c*,*e*) and desorption (panels *b*,*d*,*f*).

two aspects. In the first place, desorption and reusability of these adsorbents should be investigated. In our desorption procedure, the NiO, ZnO and CoO adsorbents after Cr(VI) adsorption were firstly centrifuged from solution. After that, $1\,\mathrm{mol\,l^{-1}}$ NaOH aqueous solution was used to convert the adsorbed Cr(VI) species to soluble $Na_2CrO_4$. Finally, these adsorbents were separated by centrifugation, washed successively with distilled water and absolute ethanol, and dried in the air at 60°C for 4 h. Figure 6 shows the morphologies of these adsorbents after Cr(VI) adsorption and desorption. Obviously, the particle size and morphology of these adsorbents are virtually unchanged, and their chemical compositions (figure 7*a–c*) are also quite similar to their counterparts before Cr(VI) adsorption. This excellent retention of morphology, size and composition is of great benefit to their reusability. Figure 7*d* shows the equilibrium adsorptive experiments at 298 K for six cycles of desorption–adsorption process. It is obvious that the equilibrium adsorption capacity renders virtually the same values, manifesting the good reusability of our adsorbents in water treatment.

Additionally, the detection limit (or sensitivity) of these adsorbents is of fundamental importance in their applications. Given that the maximum contaminant level of chromium in domestic water supplies has been set by WHO as $50\,\mu\mathrm{g\,l^{-1}}$ [12], thus a set of solutions with initial Cr(VI) concentration of $50\,\mu\mathrm{g\,l^{-1}}$ were used to perform the kinetics and equilibrium adsorption study once again. It is clear from figure 8 that all of these adsorbents can still exhibit obvious adsorptive performance in $50\,\mu\mathrm{g\,l^{-1}}$ of Cr(VI) solution, revealing that their detection limit is much lower than $50\,\mu\mathrm{g\,l^{-1}}$. This is conducive to their practical water purification. Notably, the inset of figure 8 shows CoO adsorbent, being of the highest surface hydroxyl densities (figure 2*d*), exhibits the least adsorption capacity for low concentration Cr(VI) solutions. This adsorption behaviour differs significantly from the case of $100\,\mathrm{mg\,l^{-1}}$, and can

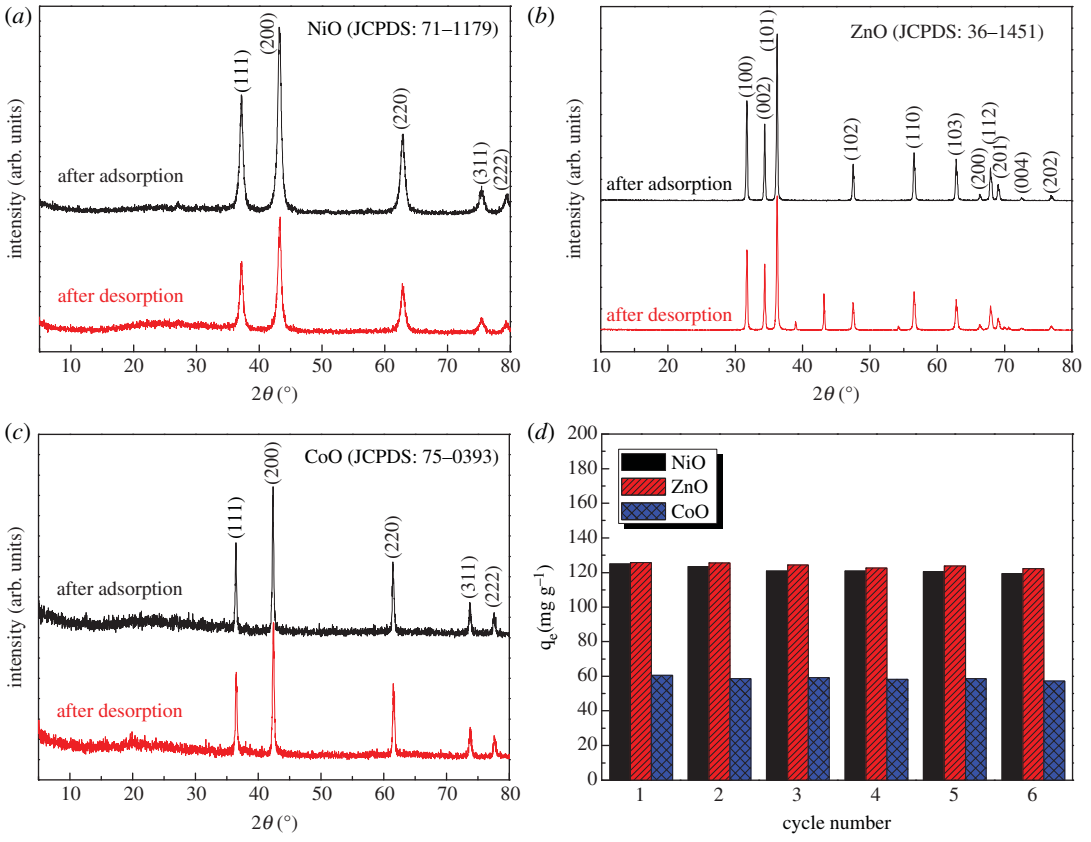


**Figure 7.** XRD patterns of (*a*) NiO, (*b*) ZnO and (*c*) CoO adsorbents after Cr(VI) adsorption and desorption. (*d*) Cr(VI) equilibrium adsorption on these adsorbents with initial Cr(VI) concentration of 100 mg $l^{-1}$ in six successive adsorption–desorption cycles at 298 K.

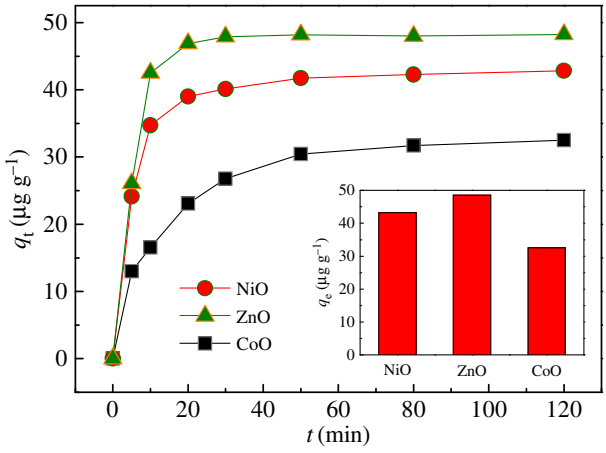


**Figure 8.** The kinetics and equilibrium (inset) of Cr(VI) adsorption on NiO, ZnO and CoO adsorbents with an initial Cr(VI) concentration of 50 μg $l^{-1}$ at 298 K.

be explained by considering the adsorption mechanism. At first, the negatively charged $Cr_2O_7^{2-}$ or $HCrO_4^-$ ions transfer to the periphery of adsorbents by electronic attraction, and then the enriched $Cr_2O_7^{2-}/HCrO_4^-$ ions will exchange with the hydroxyl groups [12] on the adsorbent surfaces to promote the adsorption process. However, if the surface hydroxyl density is extremely high in the CoO case, the initial electrostatic adsorption process is greatly inhibited, and therefore the subsequent ion exchange process is restrained. This means the proper amount of surface hydroxyl groups will be of great benefit to high adsorption capacity.

# 4. Conclusion

In summary, Chinese rose-like NiO, pinecone-like ZnO and sponge-like CoO adsorbents were synthesized by a facile and versatile urea-assisted solvothermal procedure. Their surface hydroxyl densities were determined to be 1.83, 1.32 and 4.19 mmol $[OH^-]\,g^{-1}$ for NiO, ZnO and CoO adsorbents, respectively. The presence of urea endowed the hydrothermal procedure with lower Lewis acidity, but higher concentration of surface hydroxyl groups, which would be conducive to the ion-exchange process between the adsorbents and Cr(VI) species in wastewater. The maximum adsorbed amounts of Cr(VI) were as high as 2974, 14 256 and 408 mg $g^{-1}$ for NiO, ZnO and CoO adsorbents at 298 K, respectively. Most notably, these adsorbed amounts would be greatly enhanced as increasing the adsorbing temperature. It is anticipated that this work will shed new light on the development of high-performance adsorbents.

Data accessibility. All data are provided in the main text.

Authors' contributions. J.M. designed the experiments, coordinated the study and wrote the manuscript. S.Z.-J., Y.H. and Q.S. performed the preparation experiments. Y.W., W.L. and S.S. performed the adsorption experiments. J.M., S.Z.-J., Y.H. and K.C. analysed the results. All authors gave final approval for publication.

Competing interests. The authors declare no competing interests.

Funding. This work is supported by the National Natural Science Foundation of China (NSFC no. 51472133).

# References

1. Gong JM, Liu T, Wang XQ, Hu XL, Zhang LZ. 2011 Efficient removal of heavy metal ions from aqueous systems with the assembly of anisotropic layered double hydroxide nanocrystals@carbon nanosphere. *Environ. Sci. Technol.* **45**, 6181–6187. (doi:10.1021/es200668q)
2. Li Y, Wang JD, Wang XJ, Wang JF. 2012 Adsorption–desorption of Cd(II) and Pb(II) on Ca-montmorillonite. *Ind. Eng. Chem. Res.* **51**, 6520–6528. (doi:10.1021/ie203063s)
3. Dui JN, Zhu GY, Zhou SM. 2013 Facile and economical synthesis of large hollow ferrites and their applications in adsorption for As(V) and Cr(VI). *ACS Appl. Mater. Interfaces* **5**,10 081–10 089. (doi:10.1021/am402656t)
4. Wang P, Du M, Zhu H, Bao S, Yang T, Zou M. 2015 Structure regulation of silica nanotubes and their adsorption behaviors for heavy metal ions: pH effect, kinetics, isotherms and mechanism. *J. Hazard. Mater.* **286**, 533–544. (doi:10.1016/j.jhazmat.2014.12.034)
5. Panswad T, Wongchaisuwan S. 1986 Mechanisms of dye wastewater colour removal by magnesium carbonate-hydrated basic. *Water Sci. Technol.* **18**, 139–144.
6. Ciardelli G, Corsi L, Marucci M. 2000 Membrane separation for wastewater reuse in the textile industry. *Resour. Conserv. Recycl.* **31**, 189–197. (doi:10.1016/S0921-3449(00)00079-3)
7. Körbahti BK, Artut K, Gecgel C, Özer A. 2011 Electrochemical decolorization of textile dyes and removal of metal ions from textile dye and metal ion binary mixtures. *Chem. Eng. J.* **173**, 677–688. (doi:10.1016/j.cej.2011.02.018)
8. Bilgic C. 2005 Investigation of the factors affecting organic cation adsorption on some silicate minerals. *J. Colloid Interface Sci.* **281**, 33–38. (doi:10.1016/j.jcis.2004.08.038)
9. Yu X, Liu J, Cong H, Xue L, Arshad MN, Albar HA, Sobahi TR, Gao Q, Yu S. 2015 Template- and surfactant-free synthesis of ultrathin $CeO_2$ nanowires in a mixed solvent and their superior adsorption capability for water treatment. *Chem. Sci.* **6**, 2511–2515. (doi:10.1039/c5sc00104h)
10. Roy A, Adhikari B, Majumder SB. 2013 Equilibrium, kinetic, and thermodynamic studies of azo dye adsorption from aqueous solution by chemically modified lignocellulosic jute fiber. *Ind. Eng. Chem. Res.* **52**, 6502–6512. (doi:10.1021/ie400236s)
11. Ma J, Wang Y, Liu W, He Y, Sun Q, Zuo-Jiang S, Chen K. 2015 Hundreds of milligrams of Cr(VI) adsorbed on each gram of $Cu_20$@Cu fractal structures: kinetics, equilibrium, and thermodynamics. *Cryst. Eng. Comm.* **17**, 6699–6706. (doi:10.1039/c5ce01139f)
12. Wang Y, Ma J, Chen K. 2013 Adsorptive removal of Cr(VI) from wastewater by $\alpha$-FeOOH hierarchical structure: kinetics, equilibrium and thermodynamics. *Phys. Chem. Chem. Phys.* **15**, 19 415–19 421. (doi:10.1039/c3cp52867g)
13. Alslaibi TM, Abustan I, Ahmadb MA, Foulc AA. 2013 A review: production of activated carbon from agricultural byproducts via conventional and microwave heating. *J. Chem. Technol. Biotechnol.* **88**, 1183–1190. (doi:10.1002/jctb.4028)
14. Mudhoo A, Garg VK, Wang SB. 2012 Removal of heavy metals by biosorption. *Environ. Chem. Lett.* **10**, 109–117. (doi:10.1007/s10311-011-0342-2)
15. Luo X, Zeng J, Liu S, Zhang L. 2015 An effective and recyclable adsorbent for the removal of heavy metal ions from aqueous system: magnetic chitosan/cellulose microspheres. *Bioresour. Technol.* **194**, 403–406. (doi:10.1016/j.biortech.2015.07.044)
16. Wu H, Wang T, Chen L, Jin Y, Zhang Y, Dou X. 2009 The roles of the surface charge and hydroxyl group on a Fe—Al—Ce adsorbent in fluoride adsorption. *Ind. Eng. Chem. Res.* **48**, 4530–4534. (doi:10.1021/ie800890q)
17. Cao C, Qu J, Yan W, Zhu J, Wu Z, Song W. 2012 Low-cost synthesis of flowerlike $\alpha$-$Fe_2O_3$ nanostructures for heavy metal ion removal: adsorption property and mechanism. *Langmuir* **28**, 4573—4579. (doi:10.1021/la300097y)
18. Tamura H, Tanaka A, Mita K, Furuichi R. 1999 Surface hydroxyl site densities on metal oxides as a measure for the ion-exchange capacity. *J. Colloid Interf. Sci.* **209**, 225–231. (doi:10.1006/jcis.1998.5877)
19. Zhitkovich A. 2011 Chromium in drinking water: sources, metabolism, and cancer risks. *Chem. Res. Toxicol.* **24**, 1617—1629. (doi:10.1021/tx200251t)
20. Shen H, Chen J, Dai H, Wang L, Hu M, Xia Q. 2013 New insights into the sorption and detoxification of chromium(VI) by tetraethylenepentamine functionalized nanosized magnetic polymer adsorbents: mechanism and pH effect. *Ind. Eng. Chem. Res.* **52**, 12 723—12 732. (doi:10.1021/ie4010805)
21. Kulkarni PS, Kalyani V, Mahajani VV. 2007 Removal of hexavalent chromium by membrane-based hybrid processes. *Ind. Eng. Chem. Res.* **46**, 8176—8182. (doi:10.1021/ie070592v)
22. Zavyalova U, Nigrovski B, Pollok K, Langenhorst F, Muller B, Scholz P, Ondruschka B. 2008 Gel-combustion synthesis of nanocrystalline spinel catalysts for VOCs elimination. *Appl. Catal. B: Environ.* **83**, 221–228. (doi:10.1016/j.apcatb.2008.02.015)
23. Tsoncheva T, Ivanova R, Henych J, Dimitrov M, Kormunda M, Kovacheva D, Scotti N, Santo VD, Štengl V. 2015 Effect of preparation procedure on the formation of nanostructured ceria–zirconia mixed oxide catalysts for ethyl acetate oxidation: homogeneous precipitation with urea vs template-assisted hydrothermal synthesis. *Appl. Catal. A Gen.* **502**, 418–432. (doi:10.1016/j.apcata.2015.05.034)
24. Yu XY, Xu RX, Gao C, Luo T, Jia Y, Liu JH, Huang XJ. 2012 Novel 3D hierarchical cotton-candy-like CuO: surfactant-free solvothermal synthesis and application in As(III) removal. *ACS Appl. Mater. Interfaces* **4**, 1954–1962. (doi:10.1021/am201663d)
25. Nassar NN. 2010 Kinetics, mechanistic, equilibrium, and thermodynamic studies on the adsorption of acid red dye from wastewater by $\gamma$-$Fe_2O_3$ nanoadsorbents. *Sep. Sci. Technol.* **45**, 1092–1103. (doi:10.1080/01496391003696921)
26. Zhao Y, Shen H, Pan S, Hu M, Xia Q. 2010 Preparation and characterization of amino-functionalized

nano-$Fe_3O_4$ magnetic polymer adsorbents for removal of chromium(VI) ions. *J Mater. Sci.* **45**, 5291–5301. (doi:10.1007/s10853-010-4574-5)

27. Yao X, Deng S, Wu R, Hong S, Wang B, Huang J, Wang Y, Yu G. 2016 Highly efficient removal of hexavalent chromium from electroplating wastewater using aminated wheat straw. *RSC Adv.* **6**, 8797–8805. (doi:10.1039/C5RA24508G)
28. Wan C, Li J. 2015 Facile synthesis of well-dispersed superparamagnetic $\gamma$-$Fe_2O_3$ nanoparticles encapsulated in three-dimensional architectures of cellulose aerogels and their applications for Cr(VI) removal from contaminated water. *ACS Sustainable Chem. Eng.* **3**, 2142–2152. (doi:10.1021/acssuschemeng.5b00384)
29. Sun S, Ma J, Liu W, Chen K. 2016 Gram-grade Cr(VI) adsorption on magnetite/carbon hybrid architectures. *RSC Adv.* **6**, 28 435–28 441. (doi:10.1039/c6ra01175f)
30. Zeng L, Chen Y, Zhang Q, Guo X, Peng Y, Xiao H, Chen X, Luo J. 2015 Adsorption of Cd(II), Cu(II) and Ni(II) ions by cross-linking chitosan/rectorite nano-hybrid composite microspheres. *Carbohydr. Polym.* **130**, 333–343. (doi:10.1016/j.carbpol.2015.05.015)
31. Cabatingan LK, Agapay RC, Rakels JLL, Ottens M, van der Wielen LAM. 2001 Potential of biosorption for the recovery of chromate in industrial wastewaters. *Ind. Eng. Chem. Res.* **40**, 2302–2309. (doi:10.1021/ie0008575)